Multiwavelength polarization observations of the gamma-bright quasar PKS 0420-014

I. S. Troitskiy[1], D. A. Morozova[1], S. G. Jorstad[1,2], V. M. Larionov[1], A. P. Marscher[2], I. Agudo[3], D. A. Blinov[4,1], P. S. Smith[5]

[1]Astronomical Institute of SPbSU, Russia, [2]IAR BU, USA, [3]Instituto de Astrofisíca de Andalucía, CSIC, Granada, Spain,

[4]University of Crete, Greece, [5]Steward Observatory, University of Arizona, Tucson, AZ, USA

Abstract

We analyze total and polarized intensity images of the quasar PKS 0420-014 obtained monthly with the VLBA at 43 GHz during 2008-2012, along with gamma-ray data provided by the Fermi Large Area Telescope and multi-color photometric and polarimetric measurements collected by different optical telescopes. During this period the quasar underwent a number of optical flares which were accompanied by rapid rotation of polarization angle, an increase of activity in gamma-rays, and appearance of new superluminal knots in the parsec-scale jet. We investigate the fine structure of the flares at different wavelengths and in polarized light, and determine kinematic parameters of the knots. We compare the rapid evolution of the optical polarization with the polarization of the VLBI core and knots. We interpret the multi-wavelength behavior within a model that places the blazar "dissipation zone" at the millimeter-wave core of the parsec-scale jet.

Introduction

The blazar PKS 0420-014 (z = 0.915) is active and strongly variable at all wavelengths. It is a ROSAT X-ray source [1] and was identified as a gamma-ray source by EGRET [2] and The Fermi LAT [3]. Britzen et al. [4] have found superluminal motion with $\beta_{app} \approx$ 2-14 c for five jet components (at 8.4 GHz), while Jorstad et al. [5] have measured apparent velocities of 7.6±3.5 and 10.9±2.8 at 43 GHz. The jet of 0420-014 changed its direction significantly at 43 GHz: $\Theta \approx 280°$ in 1998-2001 [5], $\Theta \approx 180°$ in 2005 [6] and $\Theta \approx 100°$ from 2008 to the present (BU group's VLBA-monitoring). In addition, a weak region of emission at 43 GHz is always visible at $\Theta \approx 180°$. At 15 GHz the jet has $\Theta \approx 200°$ and is curved toward the east, while on kiloparsec scales the jet points directly toward the south, where two lobes are apparent (1.4 GHz, [7]).

Observations and data reduction

We obtain optical (R-band) flux densities from photometric observations at the 0.4 m telescope of St. Petersburg State U. (LX200) and 0.7 m telescope of the Crimean Astrophysical Observatory (AZT-8). The data analysis for these telescopes is described in [8]. We also use R-band data carried out with the Perkins Telescope (BU group [9]), Liverpool Telescope, Calar Alto Telescopes [10] and Steward Observatory [11].

We use total and polarized intensity images of the quasar obtained by the Boston U. group at 43 GHz with the VLBA. We have modelled the maps in I, Q and U Stokes parameters by circular components with Gaussian brightness distributions to obtain total flux densities, fractional polarization, electric vector position angles (EVPA), and relative (to the core) positions of the components. The «core» is a stationary feature located at one of the ends of the portion of the jet that is visible at 43 GHz. Identification of components across the epochs is based on analysis of their distance from the core, flux density, position angle and size. We have computed the kinematic parameters of knots (proper motion, velocity, and acceleration) by fitting the positions of a component over epochs by different polynomials of order from 1 to 4 in the same manner as described in [5].

We use total flux and polarization data of UMRAO, OVRO and SMA at cm- and mm-wave radio bands to supplement our light curves.

We have derived 0.1-200 GeV gamma-ray flux densities using the data provided by the Large Area Telescope (LAT) of the Fermi Gamma-ray Space Telescope. We have used the unbinned likelihood analysis method implemented in the standard Fermi Science Tools software [12] for data reduction. The gamma-ray light curve is constructed with a 7 day integration time and with a detection criterion that the maximum-likelihood test statistic (TS) should exceed 10.0.

Results and Discussion

Light curves.

Since the beginning of the Fermi LAT observations there were two periods of enhanced activity separated by a long quiescent state in gamma rays and optical light. The active periods are characterized by a number of individual flares, increase of the degree of polarization, fast rotation of the EVPA, and appearance of new knots in the parsec-scale jet. The light curves and polarization parameters vs. time curves during the period from August 2008 to February 2013 are presented in Figs. 2. The flux density peaks are very sharp at both gamma-ray and optical wavelengths. During the largest flare (MJD 56151.5) the R band flux changes from 6.1 mJy to 3.7 mJy over a two-day interval. A cross-correlation analysis of the optical and gamma-ray data does not show any significant lag between variability in these bands (Fig. 1). Light curves for 230, 14.5, and 8.0 GHz radio bands and VLBA core at 43 GHz are more smooth, but in general replicate the long-term behavior at optical and gamma-ray wavelengths.

In addition to the long-term synchronous activity across the whole electromagnetic spectrum, a number of short synchronous flares are apparent at gamma-ray and optical wavelengths. The local maxima in gamma-rays are marked in Fig. 2a by the vertical gray solid lines. The majority, if not all, of these local peaks have counterparts in R band when optical data are available. The 7-day gamma-ray binning limits the specification of peak positions.

Table 1. Positions of flux peaks in gamma-ray, optical R, and 1 mm radio bands

Peak in gamma		Peak in optical R band		Modelled peak in 1mm radio band	
MJD	Flux (ph cm^{-2} s^{-1})	MJD	Flux (mJy)	MJD	Flux (Jy)
55085.5	2.22e-7 ± 3.52e-9	55082.9	1.500 ± 0.023	55086.4 ± 4.4	4.98 ± 0.25
55141.5	2.35e-7 ± 1.24e-9	55150.5	1.571 ± 0.007	55134.6 ± 12.5	4.92 ± 0.25
55190.5	4.26e-7 ± 6.58e-9	55193.4	1.742 ± 0.027	55194.5 ± 21.5	4.72 ± 0.26
55218.5	5.01e-7 ± 1.01e-8	55218.3	5.188 ± 0.153		
55232.5	4.03e-7 ± 6.71e-9	55233.2	3.596 ± 0.073		
55253.5	1.95e-7 ± 2.52e-9	55254.2	0.954 ± 0.042	55253.5 ± 3.5	4.04 ± 0.23
55778.5	1.52e-7 ± 2.32e-8	55778.7	1.118 ± 0.011		
55792.5	2.19e-7 ± 3.59e-10	55789.6	0.815 ± 0.024		
55813.5	1.55e-7 ± 1.35e-8	55812.5	0.635 ± 0.005		
55841.5	2.58e-7 ± 3.33e-9	55838.5	1.402 ± 0.009		
55883.5	2.97e-7 ± 4.75e-9	55886.5	1.213 ± 0.003		
55925.5	2.50e-7 ± 3.16e-9	55929.3	1.127 ± 0.015		
55967.5	2.28e-7 ± 3.20e-8	55967.4	0.941 ± 0.022		
56149.5	2.87e-7 ± 4.01e-9	56151.5	6.123 ± 0.011		
56163.5	2.82e-7 ± 1.04e-8	56161.5	4.023 ± 0.015		
56177.5	1.51e-7 ± 5.72e-9	56178.6	2.117 ± 0.012		

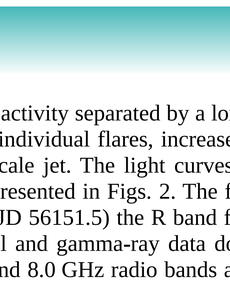

Figure 1. Discrete correlation function for gamma-ray and optical R-band data

The positions of the local gamma-ray and optical R-band peaks in flux are presented in Table 1. The mean lag time between the bands is 0.7 ± 3.0 days, which is within the integration interval for gamma-rays. As in the general correlation, there is no apparent significant lag between the sharply defined flares in the light curves.

The flux at the mm- and cm-wavelengths changes more smoothly than at higher energies. A cross-correlation analysis between the radio and optical light curves reveals a peak which is statistically significant but wide due to this long-term variability. We have applied the method proposed by Valtaoja et al. (1999) [13] to study short timescale variability at 1 mm. We have fitted flares in the 1 mm light curve by a sum of four components with an exponential rise and decay. The resulting model curve is presented in Fig. 2c by the black solid line. The time of these four peaks coincides with the local peaks of the gamma-ray and optical light curves within 1-7 days. Short timescale variability at 2 cm is less prominent. Local peaks of the 8 GHz light curve are not aligned with peaks of the gamma-ray and optical light curves.

Polarization.

Over the presented interval of observations the quasar PKS 0420-014 displays significant variability of the degree of optical polarization and a large span of EVPA rotation. During the highest gamma-ray flux maximum we observe a very high degree of the optical polarization, more than 35 %.

The activity at optical and gamma-ray wavelengths fades during the period from August 2010 to June 2011, and the degree of optical polarization differs significantly from the period of high activity. The histogram in Fig. 3 shows that only 12.5 % of points have polarization degrees > 10 % during the quiescent state, while for the first flaring period more than 70 % of points have polarization degrees > 10 %, with 66 % of the points exceeding the 10 % level for the second activity period.

The degree of polarization at radio bands 8.0 GHz and 14.5 GHz changes from < 1 % to 4-6 % during the maxima. An exception is the single point at 14.5 GHz with a polarization of 9.16 % at MJD 55621.5. This point corresponds to a rapid increase of the degree of polarization in R band, from 7-8 % to 19.2 %.

The EVPA at the optical and radio wavelengths does not show a tight connection in general, however during the interval from MJD 55080 to 55280 the difference between the EVPAs at the optical band and VLBA core at 43 GHz was consistently close to 90 degrees. During the time period from MJD 55534 to 55596 the EVPA of the VLBA core shows a synchronous rotation along with the optical EVPA, similar to that found by D'Arcangelo et al., 2007 [6].

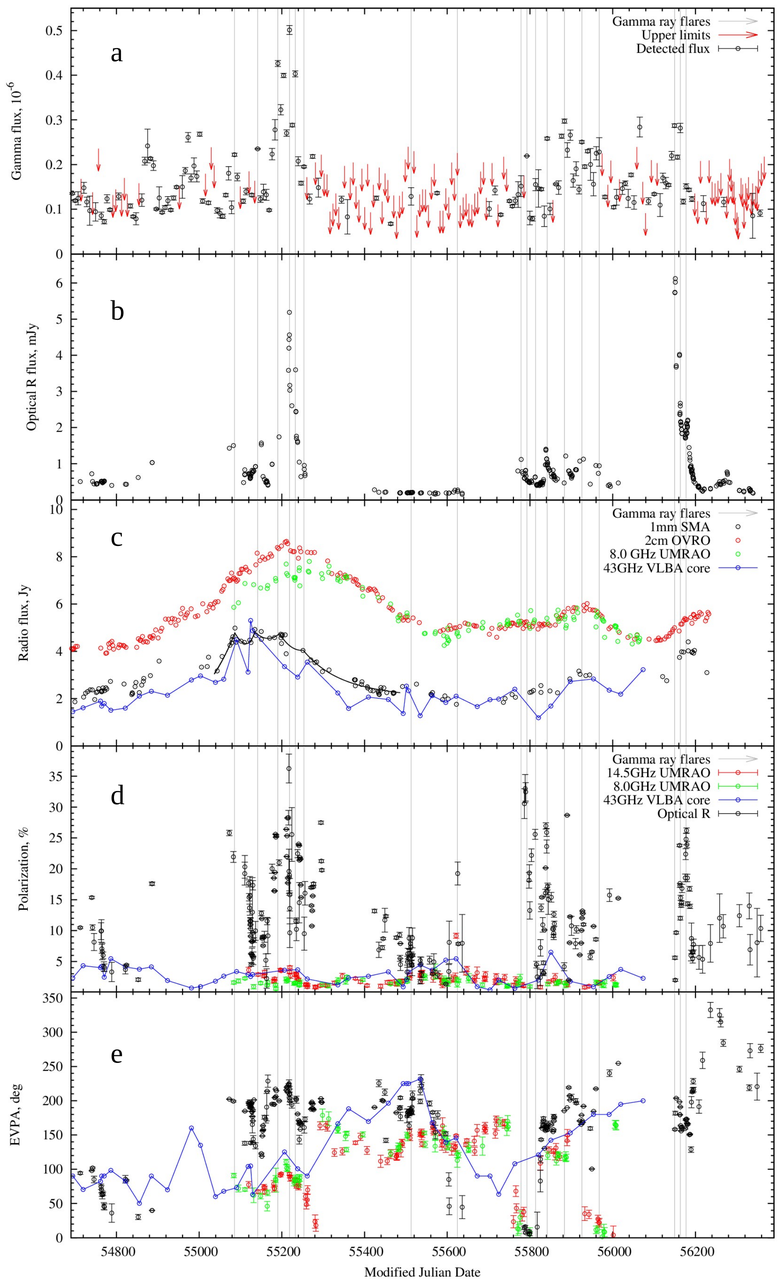

Figure 2. Light curves and polarization parameter curves.
a. Gamma-ray light curve in units of ph·cm^{-2}·s^{-1} Red arrows mark upper limits.
b. Optical light curve in R band.
c. Light curves in radio bands at 230, 15, and 8.0 GHz, and 43 GHz for the VLBA core. The black solid line shows a model of four flares at 1 mm by components with exponential rise and decay
d. Degree of polarization at 14.5 GHz and 8.0 GHz, in the 43 GHz VLBA core, and optical R band
e. EVPA at 14.5 GHz and 8.0 GHz, in the 43 GHz VLBA core, and optical R band.

VLBA images.

The parsec-scale jet of the quasar is strongly dominated by the VLBI core, which has a complex polarization pattern (see Figs. 2d, 2e), implying multi-component sub-structure in the core region. We have detected 8 moving components with apparent velocities from 6.8c to 25.3c. The parameters of these components are presented in Table 2. The VLBA image (epoch Nov. 2010) with the trajectories of the components overlaid is shown in Fig. 4. The light curve of the VLBI core at 43 GHz is similar to the light curve at 1 mm, with decays during the emergence of new components.

Table 2. Parameters of the knots.

Knot	β_{app} (c)	μ (mas/yr)	T_{eject} (Yr)	T_{eject} (MJD)
K1	6.75 ± 0.18	0.142 ± 0.004		
K2	13.43 ± 3.35	0.282 ± 0.070		
K3	16.58 ± 1.39	0.348 ± 0.029	2009.444 ± 0.110	54994 ± 40
K4	13.08 ± 1.48	0.274 ± 0.031	2009.892 ± 0.030	55161 ± 11
K5	25.30 ± 0.49	0.531 ± 0.010	2010.247 ± 0.004	55286 ± 1
K6	11.55 ± 0.72	0.242 ± 0.015		
K7	12.99 ± 1.03	0.272 ± 0.022	2010.990 ± 0.013	55564 ± 5
K8	9.08 ± 0.29	0.190 ± 0.006	2011.385 ± 0.018	55702 ± 7

β_{app} — apparent velocity, c, μ — angular speed, mas/yr

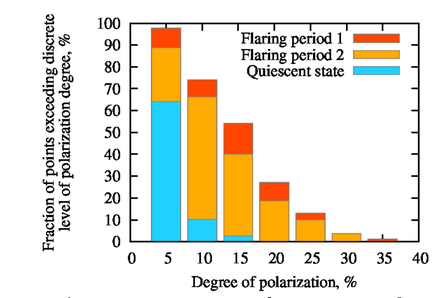

Figure 3. Percentage of points exceeding discrete levels of polarization degree in optical R band for the following three periods:
Flaring period 1 MJD 55073 — 55297
Quiescent state MJD 55424 — 55637
Flaring period 2 MJD 55787 — 56196

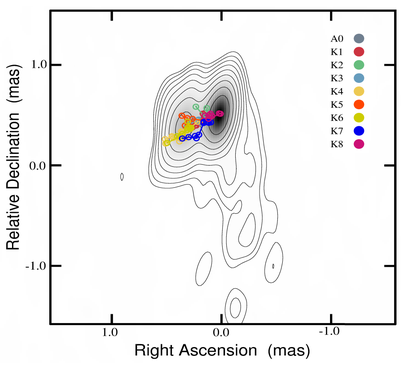

Figure 4. VLBA-map of the quasar at 43 GHz overlaid with trajectories of the knots

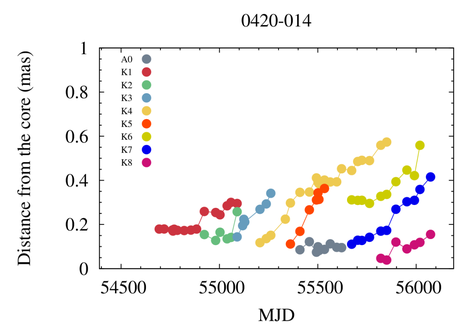

Figure 5. Position of knots in the jet with respect to the core as a function of time.

The ejection time of knot K3 (MJD 54994) is close to the peak in gamma-ray flux (MJD 55001.5). The ejection time of knot K4 (MJD 55161) corresponds to a period from 55150 to 55176 that includes a fast EVPA rotation, rising degree of polarization in optical R band, and flares in gamma-ray and optical bands. The ejection time of knot K5 (MJD 55286) corresponds to a fast rise in degree of optical polarization from 10.7 % (MJD 55273) to 27.5 % (MJD 55295). The ejection time of component K7 (MJD 55564) is close to the local peak in gamma-ray flux (MJD 55575). Synchronous rotation of the EVPA in the VLBA core at 43 GHz and optical R band from MJD 55536 to MJD 55596 was observed as component K7 passed through the core.

Summary

During the period from August 2008 to February 2013 a number of flares occurred in PKS 0420-014 from radio to gamma-ray wavelengths. We compare the light curves across the electromagnetic spectrum and find no significant lag between gamma-ray and optical R-band flux variation. Short flares in the optical and gamma-ray light curves coincide within 0.7 ± 3.0 days, which is less than the 7-day integration interval for the gamma-ray data. The times of the four peaks modelled in the 1 mm SMA light curve coincide with the corresponding gamma-ray peaks within 1-7 days.

We have detected 8 new superluminal knots in the parsec-scale jet at 43 GHz. Apparent speeds of the knots range from 6.8 c to 25.3 c. The ejection times of knots K3, K4, K5 and K7 are close to the times of gamma-rays and/or optical flares, and to intervals of significant EVPA rotations and variations in degree of polarization.

We infer from the behavior of the multi-wavelength flux and polarization that the gamma-ray and optical events are co-spatial, and that the majority of these flares occur in the vicinity or downstream of the mm-wave VLBI core [14].

Acknowledgments

We thank M. Aller for access to the UMRAO data. Also we acknowledge The Owens Valley Radio Observatory (OVRO) for online-data access. The Submillimeter Array is a joint project between the Smithsonian Astrophysical Observatory and the Academia Sinica Institute of Astronomy and Astrophysics, and is funded by the Smithsonian Institution and the Academia Sinica. The research at St. Petersburg State University was partly funded by RFBR grants 12-02-31193 and 12-02-00452. The VLBA is an instrument of the National Radio Astronomy Observatory, a facility of the National Science Foundation operated under cooperative agreement by Associated Universities, Inc. The research at Boston U. was partly funded by NASA Fermi Guest Investigator grants NNX08AV65G and NNX10AO59G. Paul Smith acknowledges funding support from NASA Fermi Guest Investigator grants NNX08AW56G and NNX09AU93G. I. Agudo acknowledges funding support from the Spanish Ministry of Economy and Competitiveness and the Regional Government of Andalucia grants AYA2010-14844 and P09-FQM-4784.

References

[1] Brinkmann, W., et al., 1994, A&A, 281, 355
[2] Fichtel, C. E. et al. 1994, ApJS, 94, 551
[3] Abdo, A. A. et al., 2010, ApJS, 188, 405A
[4] Britzen, S., et al., 2000, A&A, 360, 65B
[5] Jorstad, S. G., et al., 2005, AJ, 130, 1418-1465
[6] D'Arcangelo, F. D., et al., 2007, ApJ, 659, L107-L110
[7] Cooper, , N. J., et al. 2007, ApJ Supl 171, 376
[8] Larionov, V.M., et al., 2008, A&A, 492,389L
[9] http://www.bu.edu/blazars/VLBAproject.html
[10] http://www.iaa.es/~iagudo/research/MAPCAT/MAPCAT.html
[11] http://james.as.arizona.edu/~psmith/Fermi
[12] Atwood, W. B., et al., 2009, ApJ, 697, 1071A
[13] Valtaoja, E., et al. 1999, ApJS, 120, 95
[14] Marscher, A.P., & Gear, W.K., 1985, ApJ, 298, 114-127

Please visit our website :)

http://lacerta.astro.spbu.ru/?q=program